Proceedings of the ASME 2015 Conference on Smart Materials, Adaptive Structures and Intelligent Systems SMASIS2015

September 21-23, 2015, Colorado Springs, Colorado, USA

SMASIS2015-8835

UNDERSTANDING THE RELATIONSHIP BETWEEN PITCH AGILITY AND PROPULSIVE AERODYNAMIC FORCES IN BIO-INSPIRED FLAPPING WING VEHICLES

Zohaib Hasnain

University of Maryland College Park, MD, USA

James E. Hubbard, Jr. University of Maryland College Park, MD, USA

Joseph Calogero

Pennsylvania State University University Park, PA, USA

Mary I. Frecker

Pennsylvania State University University Park, PA, USA

Aimy A. Wissa

University of Illinois Champagne, IL, USA

ABSTRACT

Ornithopters, or flapping wing mechanical birds, represent a unique category of aerial vehicles that fill a need for small-scale, agile, long range, and payload-capable flight vehicles. This study focuses on understanding the relationship between the propulsive aerodynamic forces and pitch agility in these flapping wing vehicles. Using analytical methods, the aerodynamic moment acting upon a wing undergoing elastic flapping was calculated. A method to determine the pitch stiffness of the vehicle was then derived using a preexisting stability analysis. This method was used to demonstrate that pitch agility in flapping wing birds is intricately tied to the flapping cycle with different parts of the cycle creating stabilizing and destabilizing effects. The results indicated that pitch agility, and propulsive force generation, have a dependency on the shape of the wing, and that deformations such as bend and sweep are capable of making the vehicle more agile. Contactaided compliant mechanisms with nonlinear stiffness were designed and inserted into the wing of an ornithopter to induce controlled morphing. These elements have varying stiffness during the upstroke and downstroke parts of the cycle which introduces an asymmetry between the two halves of the flapping cycle. The resulting flapping motion exhibited a two fold increase in horizontal propulsive force over the baseline case. A motion tracking system was used to capture the free flight response of the ornithopter in steady level flight. This information was then used to calculate the pitch stiffness of the ornithopter with a rigid spar, and, one with a nonlinear compliant element inserted into the spar to induce a desired shape change. The results revealed that an upstroke in which the aerodynamic forces are similar in magnitude to that of the downstroke, may be necessary to make the vehicle more agile, and, that there is a compromise between vehicle agility and flight propulsive forces.

NOMENCLATURE

 α = Pitch angle

 α_w = Section angle of attack ϕ = Local bending angle

 φ = Included angle between flapping and flow vector

 $\omega_t = \text{Flapping angular velocity} \\
\theta = \text{Local sweep angle} \\
\gamma = \text{Forward flight inclination} \\
\gamma_w = \text{Forward inclination angle} \\
A = \text{Amplitude of oscillation}$

 $a_{r,t}$ = Element sections lift curve slope

CS = Compliant spline

 C_m = Pitching moment coefficient

 $C_{M_{ac_{r,t}}}$ = Non-dimensional moment coefficient

 c_r = Normalized chord length d = Linear displacement dr = Blade element thickness

F = Spring force

 F_w = Instantaneous aerodynamic resultant force

I = Moment of inertia J_t = Advance ratio K_{Pitch} = Pitch stiffness

 M_w = Net resultant aerodynamic moment

 M_{ac} = Applied pitching moment about aero center

k = Spring constant

q = Instantaneous pitch rate

R = Wing length

r = Element distance from the wing root

SUAS = Small unmanned aerial systems

Time index Start time t_0 Termination time

UAV = Unmanned aerial vehicle

Forward component of the flight velocity

Instantaneous flow vector V_{w} Wing element index w

Aerodynamic center x-coordinate x_w Aerodynamic center z-coordinate Z.w

INTRODUCTION

The Northern Goshawk, Accipiter gentilis, is a medium size bird of prey known for its capability to fly through cluttered woodland environment with great precision and speeds of up to 40 mph [1]. They are known for their exceptional maneuverability and rapid turn of speed capabilities. A recent documentary produced by the BBC [1] tested the flight capabilities of the Goshawk and concluded that it was capable of morphing its wings in flight, in some cases to extremely unconventional shapes. A qualitative analysis of high-speed video footage of Goshawk flight was used to determine that the remarkable maneuverability of the Goshawk was in part a result of these wing morphing capabilities. While some studies have attributed the flight capabilities to the path planning strategies [2] used by the bird, the fact remains that modern manned and unmanned small unmanned aerial systems, whether fixed or rotary wing, are currently far from the performance level associated with these biological fliers. Flapping wing vehicles, or ornithopters, most adequately satisfy a class of missions that do not require long range, but demand high agility, maneuverability, and speed. Unlike fixed wing vehicles, ornithopters do not suffer drag penalties at low speeds and smaller scales. Flapping wing flight benefits from unsteady fluidic phenomenon, such as leading edge vortices, which enhance the lift production capacity of the wing [3]. They have the ability to cruise, hover, and perch efficiently, all while remaining stealthy due to the benefit of mimicry of the common avian flier [4]. The core rationale behind using ornithopters is the fact that they provide a unique balance of the three desirable qualities of SUAS: adaptability over a wide range of missions, efficient flight at low speeds and small Reynolds numbers, and high degree of maneuverability. Avian-scale flapping flight is efficient at low Reynolds numbers and enables long-range capabilities while offering agility benefits and payload increases. The concept of wing morphing is frequently employed by natural flyers such as birds to improve performance while flying under varying circumstances. Avian fliers often alter the shape of the wing in a manner that enhances their flight efficiency or maneuverability [5]. In addition to the Goshawk, other fliers such as bats are capable of extreme wing morphing as well as asymmetric wing flapping, which allows them achieve levels of agility and maneuverability traditionally not seen in animals of their size [6]. The relationship between agility and morphing can be better understood by analyzing the wing kinematics of bat flight [7]. By combining their flapping and morphing motions bats are capable of achieving a high degree of agility [8]. Wing morphing in biological fliers is achieved through active mechanisms which involve a series of bone joints and muscles spread throughout the wing [4]. Inducing wing morphing has been a subject of much research done on ornithopters. Active mechanisms involving multi-bar linkages and smart materials have previously been explored [9]. Conn et al [10] developed a system that was capable of inducing effective morphing, however the weight added to the vehicle washed out any advantages of the induced shape change. Other work performed on developing active shape inducing mechanisms has yielded many novel designs, however, none were flight worthy considering the weight penalty [11] [12].

The goal of this study was to analyze and understand the aspects of flapping wings kinematics and wing morphing that, in turn, lead to vehicles that are agile and efficient in design. This study expands on previous research done by Wissa [4], who altered the kinematic and dynamic behavior of a flapping wing through the insertion of a passive mechanism in one of the structural members that composed the wing frame. The new design was shown to have significantly improved aerodynamic properties. Flapping efficiency was greatly improved through a substantial increase in the propulsive forces associated with the flapping motion. The fundamental focus of this research is to understand the effect of the increased aerodynamic force generation on the agility of the vehicle.

DEFINING PITCH AGILITY

In order to understand the effect of shape change on agility, it was necessary to obtain an agility metric to quantify it. Agility has traditionally been defined and quantified by different institutions in a manner that best suits their needs [13]. From a mathematical perspective, Bitten [14] defined aircraft agility as second order time rates of change of specific elements of the state vector. The choice of agility metric for the ornithopter was constrained based upon the availability of control surfaces for motion in pitch and yaw directions only. The pitch degree of freedom was chosen based on an initial analysis that revealed substantial gains in angular rates were possible without having to alter the size of the control surface. The analysis also suggested that exploiting the plant dynamics rather than increasing the size of a control surface can improve agility, thus suggesting that aerodynamic force generation may not be the only factor involved in determining vehicle agility. Based upon the mathematical definition of agility provided by Bitten, the average pitch rate was selected as the starting point for the analysis (Equation 1). Here, q represents the instantaneous pitch rate, and t_0 and t_f represent the start and termination time, respectively, of any initiated pitching maneuver.

 $Average\ Pitch\ Acceleration = \frac{\int_{t_0}^{t_f} (Pitch\ Acceleration) dt}{t_f - t_0}$

$$=\frac{\int_{t_0}^{t_f} \dot{q} dt}{t_f - t_0} \tag{1}$$

For a vehicle undergoing steady level flight, the relation between pitch acceleration and net applied aerodynamic moment is given by Equation 2.

$$\dot{q} = \frac{M}{I_{YY}} \tag{2}$$

Where M is the net resultant aerodynamic moment, and I_{YY} is the moment of inertia. The average pitch rate can thus be altered by varying the net resultant moment that is acting on a flier at any given instant. It will be shown in the subsequent section that M is a function of the vehicle dynamics and kinematics. For now, the important observation is the fact that the net aerodynamic moment acting on a body is responsible for making the vehicle more or less agile.

AGILITY AND FLIGHT VEHICLE PHYSICS

Agility in all manner of fliers is intricately tied to the associated plant physics of the vehicle. This fact has been used extensively in the design of highly agile fixed wing vehicles. The net aerodynamic moment experienced by a flier can be related to the effective angle of attack, α through the relation expressed in Equation 3.

$$M = K_{Pitch}\alpha \tag{3}$$

The term K_{Pitch} is the Pitch Stiffness of the flier. A simple linear analogy can now be used to better understand the concept of modifying pitch agility through plant dynamics. For a linear spring, the force that is exerted in response to a prescribed displacement is given by F = -k d where k is the spring constant or stiffness, and d is the displacement. The negative sign before the stiffness term indicates that force is a restoring force, and that the displaced node attempts to return to equilibrium position under the influence of this force. In the absence of this negative sign, the force would not be a restoring force and the response of the spring to any prescribed input would be divergent. For a flapping wing vehicle, the sign of the restoring force in response to any given pitch input could determine whether the resultant moment is divergent or not. In the event that it is, a small input in pitch, could lead quickly to a large applied aerodynamic moment. In terms of stability this corresponds to a design that is unstable when flying without feedback control.

Mathematically, the pitch stiffness can be defined as the rate of change of resultant moment on an aerial vehicle with respect to the pitch angle. From a physical perspective, it is the sign of the pitch stiffness instead of the absolute value that effects the plant physics. The simplified cases for positive, zero, and

negative pitch stiffness are shown in Figure 1. The schematics illustrate in a general sense how the moment coefficient, C_m , depends on the pitch angle of the vehicle, a. For positive pitch stiffness values, an increase in pitch angle leads to an aerodynamic moment that creates a displacement in the same direction as the original disturbance. Any disturbance therefore leads to a moment that increases consistently, causing the pitch angle to increase divergently. This particular plant dynamic is unstable, and requires closed loop control in the form of a pilot or flight computer for stabilization. For the case of zero pitch stiffness, there is no resultant aerodynamic moment other than the zero angle of attack moment. Any pitch disturbance, therefore, continues to grow at a constant rate. Lastly, for the case of negative pitch stiffness, the resultant aerodynamic moment is always restoring, i.e. it will act in a direction opposite to the disturbance and return the vehicle to its equilibrium state. This relationship is representative of a stable plant, with which most modern aircraft are designed. A depiction of the effect of these three cases of pitch stiffness is also shown in Figure 2. For fixed wing aircraft, the pitch stiffness is a function of the location of the aerodynamic center with respect to the center of gravity of the vehicle, the location of which remains relatively unchanged during flight. For flapping wing type small UAV, the pitch stiffness varies continuously and periodically through the flap

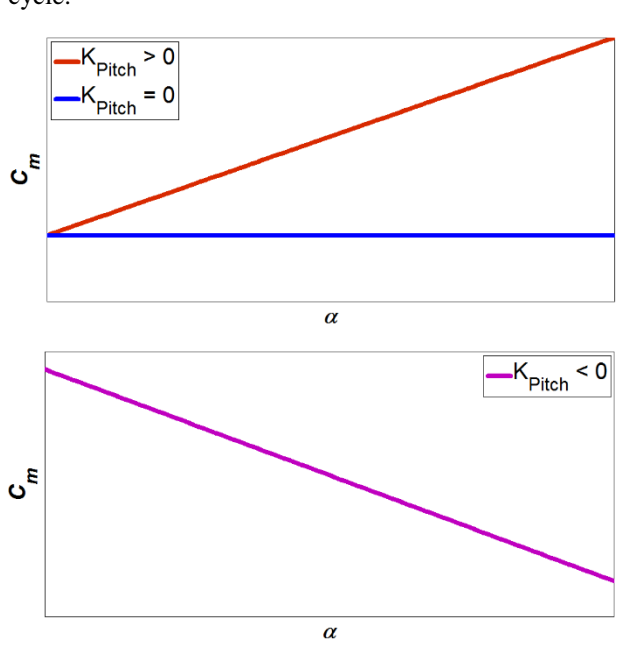


Figure 1. Schematic illustration of moment coefficient dependency on angle of attack for positive or zero pitch stiffness (top) and negative pitch stiffness (bottom)

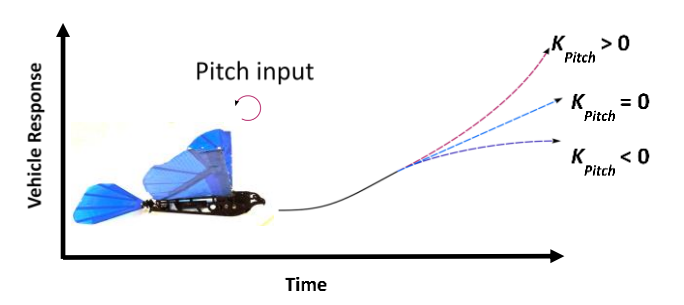


Figure 2. Illustration of vehicle response for three different cases of pitch stiffness

UNDERSTANDING THE PITCH STIFFNESS

As part of a stability analysis performed on flapping wing type vehicles, Taylor and Thomas [15] developed a method to calculate the pitch stiffness using a quasi-static method using blade element theory. Their model was limited to rigid flapping wings. It was thus modified to incorporate the effect of bending. Starting with a blade element of thickness dr, and distance r from the root of the wing (shown in Figure 3), the moment exerted due to aerodynamic loads was calculated. The resultant aerodynamic moment acting upon the element can, therefore, be calculated through a summation of the loads shown in the figure.

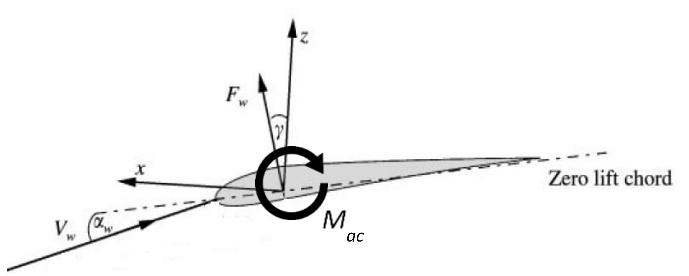


Figure 3 Taylor and Thomas's [15] blade element force diagram

The expression for the moment is given by Equation 4. The subscripts r and t in the expression denote that the corresponding term is function of radial distance from the root and time. Here, ϕ is the local bend angle, defined as the angle between the wing neutral axis and the local vertical z axis. The local sweep angle θ is defined as the angle between the wing long axis and the local y-axis in a plane containing the flow vector. The coordinates x_w and z_w denote the location of the aerodynamic center with respect to the center of gravity of the SUAV. $F_{w(r,t)}$ is the instantaneous net aerodynamic force acting at the aerodynamic center, $V_{w(r,t)}$ is the instantaneous flow vector, $\gamma_{(r,t)}$ is the forward flight inclination angle of the force vector with respect to the local z-axis, and $\alpha_{w(r,t)}$ is the local section angle of attack defined as being positive for cases where the normal component of the flight force is positive. Any applied pitching moment is denoted by M_{ac} .

$$M_{w(r,t)} = \cos(\beta_{r,t}) * \cos(\sigma_t) * \left[x_{w(r,t)} * F_{w(r,t)} * \cos(\gamma_{w(r,t)}) + z_{w(r,t)} * F_{w(r,t)} * \sin(\gamma_{w(r,t)}) + M_{ac(r,t)} \right]$$
(4)

In order to calculate the pitch stiffness, each of the terms in Equation 4 must be differentiated with respect to the pitch angle. Using blade element momentum theory to evaluate the aerodynamic loads on the body [15], the differentiation can be performed, simplifying to the expression presented in Equation 5.

$$\frac{\partial M_{w(r,t)}}{\partial \alpha_{b}}$$

$$= \frac{1}{2} \rho u_{t}^{2} a_{r,t} c_{r} R dr cos(\theta_{t}) \cos(\phi_{r,t}) \left\{ (x_{w(r,t)} \cos(\gamma_{r,t}) + z_{w(r,t)} \sin(\gamma_{r,t})) * \left[\frac{r}{J_{t}} (2\alpha_{w(r,t)} sin(\varphi) + 1) \right] + (z_{w(r,t)} \cos(\gamma_{r,t}) - x_{w(r,t)} \sin(\gamma_{r,t})) \left[\alpha_{w(r,t)} \left(1 - \frac{r}{J_{t}} \cos(\varphi) \right) \right] + C_{Mac_{r,t}} \left[2r c_{(r)} \frac{sin(\varphi)}{J_{t} a_{r,t}} \right] \right\}$$
(5)

The first term on the left hand side is the forward flight term. Here u_t denotes the forward component of the flight velocity vector, a_{rt} denotes the element sections lift curve slope, c_r is the chord length normalized with respect to the wing length R, and dr is the element thickness. Right away this leads to the important conclusion that, for any flapping wing SUAV that has zero or very small forward velocity, the pitch stiffness will be zero or very close to zero. It also suggests that any change in SUAV forward flight speed cannot change the sign of the pitch stiffness, however it can affect the magnitude of it.

The forward flight term is followed by the bending and sweep terms $(cos(\sigma_t) \ and \ cos(\beta_{r,t}))$. Based on the way the bend and sweep angles are defined, their values always stay between $-\pi/2$ and $\pi/2$. This means that, for any bending or sweep that does induce a significant change in the location of the center of gravity, the sign of the pitch stiffness may not be altered. For such a case, the bend and sweep may again only alter the magnitude of the pitch stiffness.

The final term, in the square brackets, is the shape change term that we are attempting to manipulate through the installation of spatially distributed compliant elements (SDCEs). In this expression, J_t represents the advance ratio and is defined as $J_t = \frac{u_t}{R\Omega_t}$, u_t is the forward component of the flight velocity, R is the length of the wing, Ω_t is the flapping angular velocity, φ represents the included angle between the flow due to flapping and the oncoming flow vector, α_b and $\alpha_{w(r,t)}$ represent the pitch angles of the overall body and local element respectively, and $C_{Macr,t}$ represents the non-dimensional moment coefficient based upon the applied pitching aerodynamic moment. Taylor

and Thomas used the expression in Equation 5, to make several observations about the pitch stiffness. Some relevant observations are summarized in the following paragraph.

The way the included angle, φ is defined, it assumes obtuse values on the downstroke and acute values on the upstroke [15]. The $\sin \varphi$ term is therefore positive throughout the cycle. The $cos \varphi$ term is positive on the upstroke and negative on the downstroke. For the downstroke, all three terms contained in the square brackets in the shape change term will thus be positive, since α is positive by definition during the downstroke. The sign of the pitch stiffness during the downstroke is then dependent upon the forward inclination angle $\gamma_{r,t}$. For the case of the downstroke during flapping this angle is always positive and usually small enough to ensure that the overall pitch stiffness is negative provided that the aerodynamic center lies far enough behind and/or above the center of gravity. In other words, under most circumstances the sign of the pitch stiffness during the downstroke part of the cycle is solely governed by the location of the aerodynamic center with respect to the center of gravity. During the upstroke, things are more complicated. The first two terms in the square brackets can now assume positive or negative values depending on ϕ and J_t . Under most circumstances these terms are small in forward flight at low velocity. For this case $\gamma_{r,t}$ is also small and positive, as is $\alpha_{w(r,t)}$ based on the way it was defined. The sign of the pitch stiffness therefore again is heavily influenced by the relative locations of the aerodynamic center with respect to the center of gravity.

We therefore conclude this section with the understanding that the relative locations of the aerodynamic and gravity (AC and CG respectively) centers of the vehicle are key in determining the sign of the pitch stiffness for most cases of flapping flight. The remainder of this effort focuses on the following:

- 1) Determining the locations of the AC and CG, and understanding how a specific induced shape change affects the locations of these two points
- 2) Understanding the balance between potential agility gains and aerodynamic propulsive force generation efficiency

The global and long term objective of this study is to provide an analytical framework that will ultimately lead to an efficient method of computing pitch stiffness for vehicles that are undergoing controlled shape change.

EXPERIMENTAL METHOD

As part of the previous half of this research effort [4], motion data for multiple, specific selected points on the wing of a flapping wing robot was collected using a VICON motion tracking system. This initial phase was oriented towards understanding the effect of shape change on propulsive force generation, and thus the marker selection was optimized towards that goal. In order to calculate the CG and AC locations of an element, one must be defined in a manner that satisfies the underlying blade element theory flow assumptions that are made

in calculating Equation 5. Figure 4 shows the original marker positions on the wing of the flight vehicle that was used for testing as well as the element allocation and selection. Markers were placed along alternating slices of the span in a manner that effectively allowed for a total of 9 possible selections for elements across the wing span.



Figure 4 Ornithopter Wing Span showing potential and selected elements and VICON markers (selected markers on the elements used for analysis are highlighted in yellow)

The three elements highlighted in red in Figure 4 are the ones that were selected for this analysis. The three elements represent three different sets of physics associated with the wing. The one that is closest to the root is subject to the smallest range of flapping motion. Any deflections associated with this part of the wing are thus expected to be small. The second element is selected to be close to the half way mark on the wing. This element is representative of the set of physics that would be associated with deformations that are not as large as those on the tip, nor as small as the ones very close to the root. And finally the third element which is placed on the wing tip captures the physics associated with the larger range of motion at this location.

The vehicle was tested in free flight conditions with the *x*-axis representing the horizontal direction of the flight and *y* and *z* axis representing the out-of-plane and vertical directions respectively. Throttle was maintained to achieve a flight profile as close to steady level as possible. Other details pertaining to the specifics of the test flights can be found in reference [4]. A total of two cases corresponding to variations of induced wing shape were tested.

The wing morphing was induced using a novel method developed as part of the broader research [9]. Passive contact-aided compliant mechanisms with non-linear stiffness were inserted into the wing leading edge spars at 37% from the wing root on both wings to mimic the wrist joints of biological fliers. Insertion of these elements allowed for the wing to fold downwards during the upstroke, effectively reducing the negative vertical force contribution of the upstroke part of the flapping cycle, and therefore increasing the flapping efficiency.

For the purposes of the current analysis two cases will be presented. The first case corresponds to a leading edge spar with no compliant mechanism inserted. This is the baseline configuration in which the wing shape during the upstroke and downstroke are very similar. The second case is that of a leading

edge spar with a compliant element that was associated with the highest value of propulsive force generation.

RESULTS AND ANALYSIS

Figure 5, Figure 6, and Figure 7 show the plots for the element time histories for the spar with no compliant mechanism, referred to as the solid spar. The history begins at one time step prior to the initiation of the upstroke, and concludes at the end of the downstroke. While an attempt was made to keep the vehicle as close to steady level as allowed by the hardware, the final data indicated that it was moderately pitched up for this case. For the element that is closest to the wing root, the first and the last marker are on spars that support the wing. At the beginning of the upstroke the element under the aerodynamic loads assumes a concave shape, as the upstroke begins to terminate the markers on the support spars slow down faster than the markers on the membrane resulting in an inflection right before the beginning of the downstroke. The process then repeats itself with the element now first assuming a convex shape at the beginning of the downstroke. Note that the marker on the trailing edge never achieves an altitude greater than the marker on the leading edge for any instance of the element history. This is due to the fact that the element is close to the root where the displacements are small and that the vehicle is pitched up.

For the mid wing location element, the behavior varies much more than the root element. The upstroke is initiated by an element that is concave in shape and the inflection is seen at the end of the upstroke, however at the beginning of the downstroke the element assumes an "S" shape. The reason why this shape is observed is because the while the 1st and 4th marker of this element are on support structures the 2nd, 3rd and 5th markers sit on membrane which during the downstroke stretches in a convex manner for markers 2 and 3, and 4 bends upwards at marker location 5.

Finally for the element closest to the wing tip, the behavior is similar with the shape being concave on the way up since the 1st and 3rd marker sit on support structures, and convex on the downstroke.

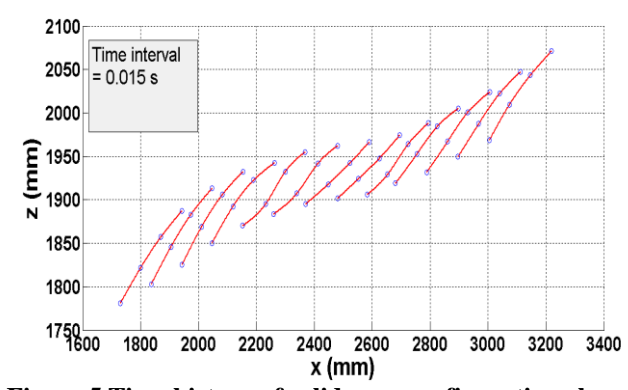


Figure 5 Time history of solid spar configuration element closest to root, shown over 1 complete cycle starting at the

initiation of the upstroke, markers were used as points fitted with a spline curve to approximate the shape of the membrane

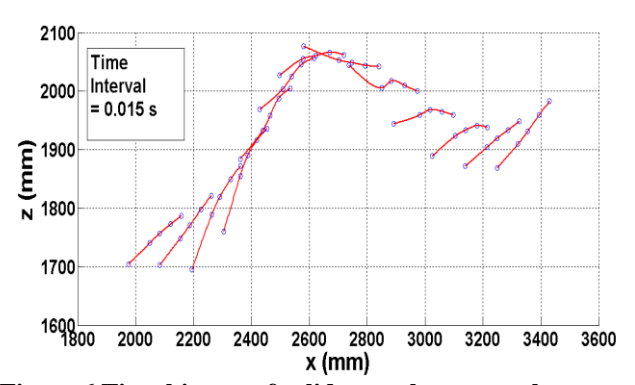


Figure 6 Time history of solid spar element at the center of the wing showing the irregular element shapes achieved at the initiation of the downstroke

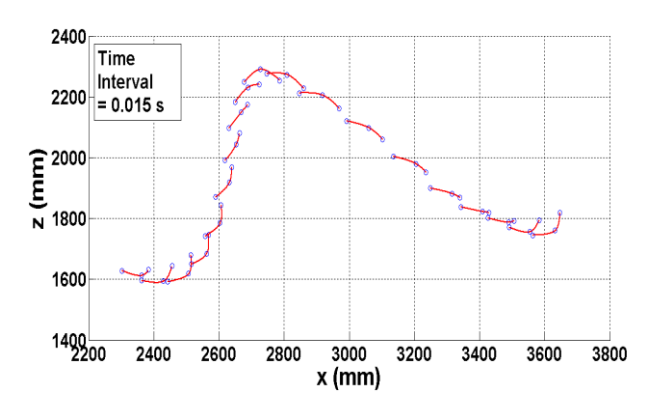


Figure 7 Time history of solid spar element at wing tip

The element shapes were then used to calculate the locations of the center of gravity for each instance by assuming that the mass of the entire element was lumped at the locations of the markers. The identification of the location of the aerodynamic center required interpolation of the data. For the cases in which the element deformations were purely concave or convex, the element was fitted with a spline curve. The aerodynamic center was then identified under the assumption that element could be represented a thin, cambered flat plate. The camber of the plate was determined by the spline interpolation between markers. For the more irregular "S" shapes a fit between the markers was determined while ignoring the contribution of the markers that were situated between support structures on membrane. One such case is shown Figure 8. The element aerodynamic center is then calculated assuming that it is a cambered flat plate. While this approximation may introduce error in the overall results, the number of instances at which it is made is small, only 5 out of 50 instances of the cycle required this treatment. A more detailed analysis of the effect of this

approximation will be a part of the extended work to be performed as part of this project.

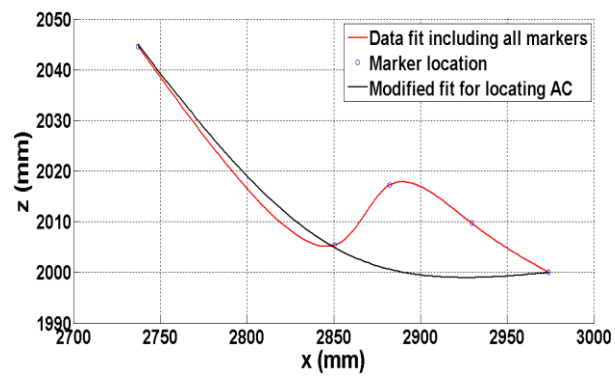


Figure 8 Comparison of approximate membrane shape with shape used in AC location identification, the effect of markers located on unsupported membrane is ignored and the membrane is assumed to be a cambered flat plate

Figure 9, Figure 10, and Figure 11 show the in-flight locations of the center of gravity and aerodynamic center, for all three elements, respectively. The criteria for having a negative pitch stiffness for small forward flight angles required that the AC be above and/or behind the CG. For all of the cases that have been presented below the AC generally lies slightly ahead and above the CG. In order to truly determine the effect on the pitch stiffness, a quantitative comparison at every time instance and its integrated effect over all time steps and elements would be required. However, a simple observation can be made based on these results. The CG and AC locations are almost always very close to one another (always within 20 mm, mostly within 10 mm). The $x_{w(r,t)}$ and $z_{w(r,t)}$ terms are therefore very small and thus any contribution from the first two terms in the curly brackets of Equation 5 is small.

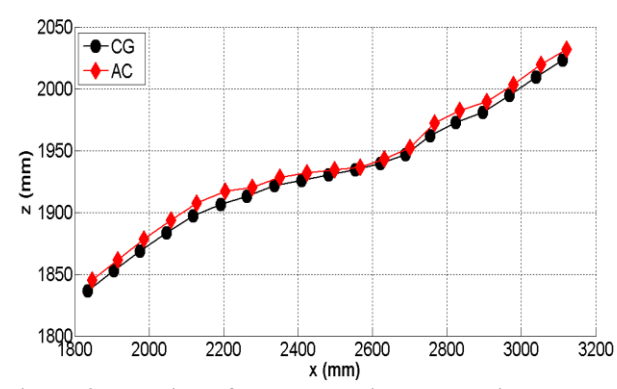


Figure 9 Location of aerodynamic and gravity centers for solid spar element closest to root for one flapping cycle, the aerodynamic centers and centers of gravity lie within 10-20 mm of one another

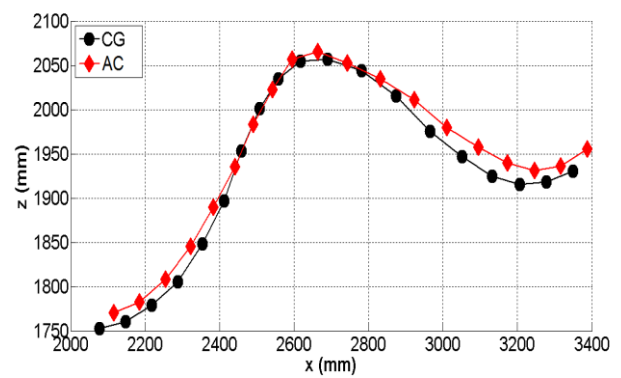


Figure 10 Location of aerodynamic and gravity centers for solid spar mid-wing element, both points lie in close proximity to one another

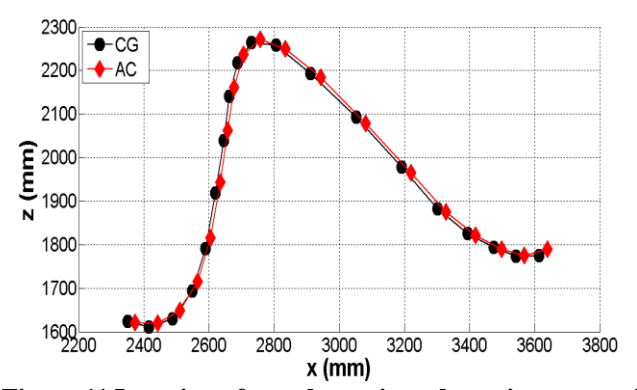


Figure 11 Location of aerodynamic and gravity centers for solid spar wing tip element

The second case that was tested is shown in the sequence of Figure 12, Figure 13, and Figure 14 below. The data shown below is for one complete cycle beginning close to the end of the downstroke. Unlike the rigid spar case, this instance of flight was much closer to level flight. The elements undergo deformations that correspond to the aerodynamic loads experienced by them during various parts of the cycle. The number of cases which exhibited irregular "S" shaped deformations was slightly fewer than the solid spar case. Even for the cases where such deformations existed, the magnitude of the irregularity was smaller. The case for the mid wing element is shown in Figure 13 with a time interval of 0.02 s, as opposed to 0.015 s for all the other cases, to reduce clutter on the plot and improve clarity in viewing the deformed element shapes. A noteworthy observation for the spar with the compliant mechanism is that a significant amount of sweep in the profile is observed compared to the solid spar case. This can be seen by the behavior of the tip element shown in Figure 14. This motion corresponds to that of natural fliers in which the tip traces out a "figure 8" asymmetric path.

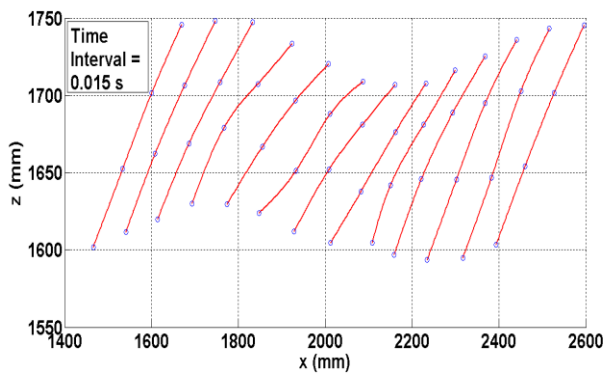


Figure 12 Time history of compliant spar configuration element closest to root, shown over 1 complete cycle starting close to the end point of the downstroke, markers were used as points fitted with a spline curve to approximate the shape of the membrane

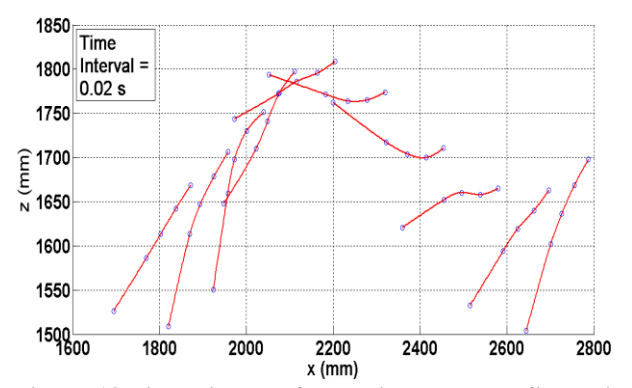


Figure 13 Time history of compliant spar configuration element located at mid-wing, some "S" shape deformities were observed however the magnitude of the deformation was in general less than that of the rigid spar case

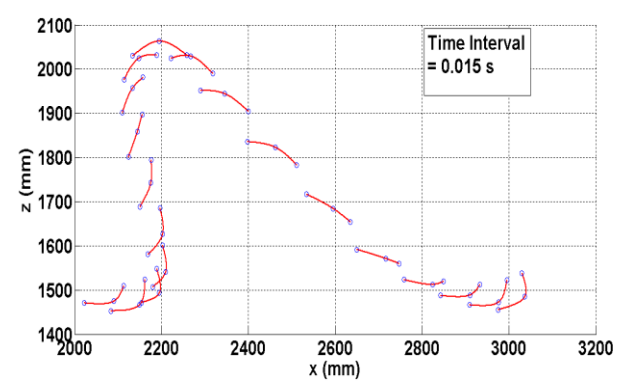


Figure 14 Time history of compliant spar configuration element located at wing tip, element deformations are similar to those observed for solid spar cases, general profile of the cycle is "swept" backwards compared to the solid spar case

Shown in the following sequence of Figure 15, Figure 16, and Figure 17 are the locations of the aerodynamic centers

and centers of gravity for each of the elements. The horizontal relative displacement between the two points is relatively small for all the cases. However, for both the element at the root and the element at mid-wing location the center of gravity lies well below the aerodynamic center. The $x_{W(r,t)}$ distance in this case will still be small, but the $z_{W(r,t)}$ term will be larger and more negative (CG below AC) than that of the solid case. This implies that for the compliant spar case, the pitch stiffness is more negative than that of the solid spar case.

In addition to the pitch stiffness for the two cases discussed in this section, the horizontal and vertical propulsive flight forces were also calculated. A relative comparison of the two cases is shown below in Table 1. The forces have been normalized by the rigid spar case for purposes of comparison.

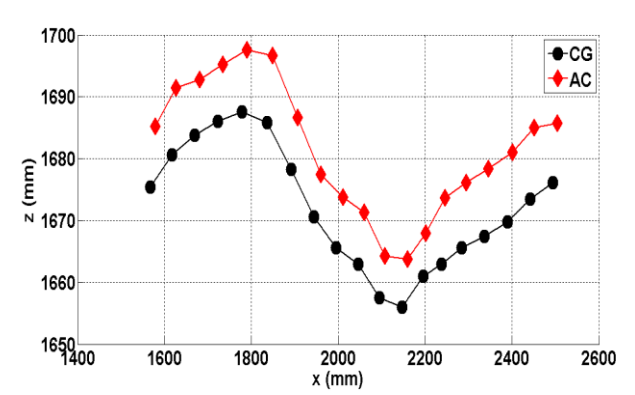


Figure 15 Location of aerodynamic and gravity centers for compliant spar element closest to root over one flapping cycle, the aerodynamic centers and centers of gravity lie significantly further apart than for the solid spar case

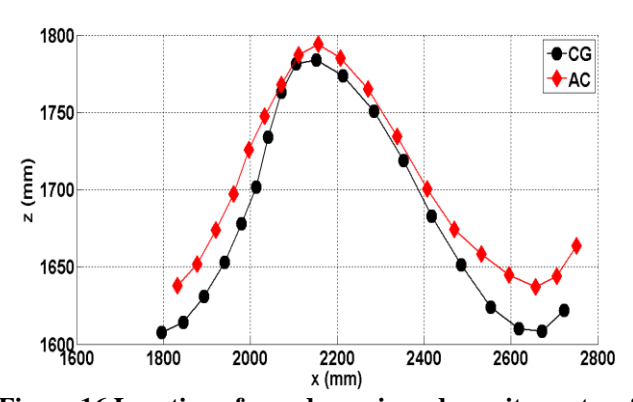


Figure 16 Location of aerodynamic and gravity centers for solid spar mid-wing element, the CG lies consistently below the AC, the two points are separated slightly more than they were for the solid spar case

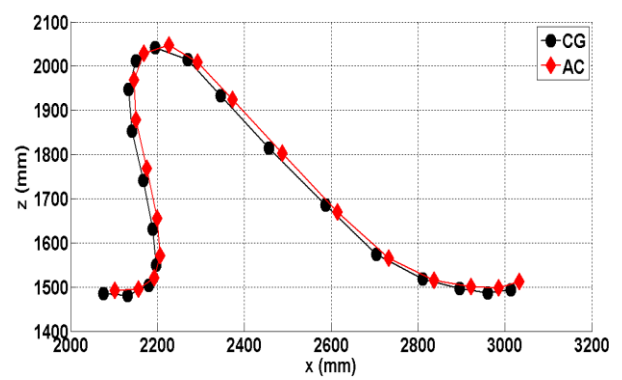


Figure 17 Location of aerodynamic and gravity centers for compliant spar wing tip element

Table 1 Flight force Comparison of solid and compliant spar configurations

Spar Configuration	Horizontal Relative Force	Vertical Relative Force
Solid	1	1
Compliant	1.98	0.7

The compliant spar produced twice the amount of propulsive horizontal thrust and required only 70% of vertical force required by the solid configuration to maintain level flight. This was achieved at identical throttle and hence, power levels, indicating that a compliant configuration increased the efficiency associated with flight. The horizontal and vertical propulsive forces were calculated using motion capture data. The details of the experiment and calculations are discussed in depth in reference [4].

SUMMARY, CONCLUSIONS AND FUTURE WORK

The goal of this research was to contribute towards the understanding of the mechanisms that potentially contribute to flapping wing vehicle pitch agility. A framework based on preexisting methods was applied, which allowed us to determine whether controlled shape change would enhance or deteriorate the agility associated with a flapping wing vehicle. The pitch stiffness was used to determine whether an induced wing shape would result in a design which was agile relative to the baseline case of no shape control. The morphing was induced using compliant elements inserted into the wing leading edge spars. The pitch stiffness was qualitatively analyzed through an understanding of its dependency on the relative locations of the aerodynamic and gravity centers of the wing.

The solid spar case revealed that the aerodynamic center lay very close to the center of gravity for all instances over the flapping cycle. In most cases, the AC actually lies ahead of and below the center of gravity. This resulted in a pitch stiffness value that was relatively positive compared to the compliant spar case. For the latter, the aerodynamic center was well above the center of gravity for all instances of flapping, at most locations

along the wing span. This led to the compliant spar design having a more negative pitch stiffness. The implications of the relative pitch stiffness values being more or less negative are directly tied to pitch agility. A more negative value of pitch stiffness corresponds to a higher value of restoring moment that the vehicle is subjected to as it attempts to pitch. The effects of relative positive pitch stiffness can be seen in the time history of the elements. For the solid spar case, the vehicle appears to be increasing in altitude i.e. pitched up. This design was extremely difficult to fly level, since any minute disturbance would to cause it to deviate in a divergent manner. Despite several attempts, none of the pilots were able to obtain data that was as steady level as the compliant design, which on the other hand was significantly easier to fly level in the first attempt.

It can therefore be concluded that from a resistive force standpoint, the solid spar configuration was the more agile design. However, it was not the most efficient. The compliant configuration resulted in twice the horizontal propulsive force and required only 70% of the vertical force of the solid design to stay aloft for the same power input. It would thus appear that there exists a compromise between how agile a design is versus how efficient it is.

This study was the first step in establishing a broader framework that will eventually allow us to compute the agility that is associated with flapping wing vehicles. While the most crucial parameters were taken into account while performing the calculations, the assumptions behind the analysis limit the model to a narrow range of flight conditions. Constraints on quantities such as the advance ratio, flight inclination angle and lifting forces are inherent, and implied in this iteration. Future work will include developing corrections that would allow for relaxation of these constraints, and computing, quantitatively, the value of the pitch stiffness for an entire vehicle as opposed to individual wing elements.

ACKNOWLEDGMENTS

The authors gratefully acknowledge the support of AFOSR grant number FA9550-13-0126 under the direction of Dr. David Stargel. The resources of the NASA Langley Research Center, The Pennsylvania State University, University of Maryland and Morpheus Lab.

REFERENCES

- [1] BBC Narture, "Northern Goshawk," 01 01 2015. [Online]. Available: http://www.bbc.co.uk/nature/life/Northern Goshawk.
- [2] S. Karaman and E. Frazzoli, "High-speed flight in an ergodic forest," in *IEEE International Conference on Robotics and Automation (ICRA)*, 2012, Saint Paul, MN, 2012.
- [3] P. Seshadri, M. Benedict and I. Chopra, "Understanding Micro Air Vehicle Flapping-Wing Aerodynamics Using Force and Flowfield Measurements," *Journal of Aircraft*, vol. 50, no. 4, pp. 1070-1087, 2013.

- [4] A. A. Wissa, "Analytical Modeling and Experimental Modeling of a Passively Morphing Ornithopter Wing," University of Maryland, College Park, 2014.
- [5] C. Thill, J. Etches, I. Bond, K. Potter and P. Weaver, "Morphing Skins," *The Aeronautical Journal*, vol. 112, pp. 117-139, 2008.
- [6] J. Colorado, A. Barrientos, C. Rossi and K. Breuer, "Biomechanics of smart wings in a bat robot: morphing wings using SMA actuators," *Bioinspiration & Biomimetics*, vol. 7, no. 3, 2012.
- [7] D. K. Riskin, D. J. Willis, J. Iriarte-Diaz, T. L. Hedrick, M. Kostandov, J. Chen, D. H. Laidlaw, K. S. Breuer and S. M. Swartz, "Quantifying the complexity of bat wing kinematics," *Journal of Theoretical Biology*, vol. 254, pp. 604-615, 2008.
- [8] J. Colorado, A. Barrientos, C. Rossi and K. Breuer, "Biomechanics of morphing wings in a Bat-robot actuated by SMA muscles," *Bioinspiration and Biomimetics*, vol. 7, no. 3, 2012.
- [9] Y. Tummala, "Design and optimization of contact-aided compliant mechanisms with nonlinear stiffness," Pennsylvania State University, State College, 2013.
- [10] A. Conn, S. Burgess and C. Ling, "Design of a Parallel Crank-Rocker Flapping Mechanism for Insect-Inspired

- Micro Air Vehicles," *Journal of Mechanical Engineering Science*, vol. 221, pp. 1211-1222, 2007.
- [11] A. Cox, D. Monopoli, D. Cveticanin, M. Goldfarb and E. Garcia, "The Development of Elastodynamic Components for Piezoelectrically Actuated Flapping Micro-air Vehicles," *Journal of Intelligent Material Systems and Structures*, vol. 13, pp. 611-615, 2002.
- [12] K. Frampton, M. Goldfarb, D. Monopoli and D. Cveticanin, "Passive Aeroelastic Tailoring for Optimal Flapping Wings," in *Fixed and Flapping Wing Aerodynamics for Micro Air Vehicle Applications*, Reston, VA, Wiley, 2001, pp. 473-482.
- [13] A. A. Paranjape and a. N. Ananthkrishnan, "Combat Aircraft Agility Metrics: A Review," *Journal of Aerospace Sciences and Technologies*, vol. 58, no. 2, 2005.
- [14] R. Bitten, "Qualitative and Quantitative Comparison of Government Agility Metrics," *Journal of Aircraft*, vol. 27, no. 3, pp. 276-282, 1989.
- [15] G. K. Taylor and A. L. R. Thomas, "Animal Flight Dynamics II. Longitudanal Stability in Flapping Flight," *Journal of Theoretical Biology*, no. 214, pp. 351-370, 2002.